JPE 17-1-28

https://doi.org/10.6113/JPE.2017.17.1.282
ISSN(Print): 1598-2092 / ISSN(Online): 2093-4718

An Enhanced Power Sharing Strategy for Islanded Microgrids Considering Impedance Matching for Both Real and Reactive Power

Liaoyuan Lin*, Qian Guo**, Zhihong Bai*, and Hao Ma†

*,†College of Electrical Engineering, Zhejiang University, Hangzhou, China
**College of Mechanical and Electrical Engineering, China Jiliang University, Hangzhou, China

Abstract

There exists a strong coupling between real and reactive power owing to the complex impedances in droop based islanded microgrids (MGs). The existing virtual impedance methods consider improvements of the impedance matching for sharing of the voltage controlled power (VCP) (reactive power for Q-V droop, and real power for P-V droop), which yields a 1-DOF (degree of freedom) tunable virtual impedance. However, a weak impedance matching for sharing of the frequency controlled power (FCP) (real power for P-ω droop, and reactive power for Q-ω droop) may result in FCP overshoots and even oscillations during load transients. This in turn results in VCP oscillations due to the strong coupling. In this paper, a 2-DOF tunable adaptive virtual impedance method considering impedance matching for both real and reactive power (IM-PQ) is proposed to improve the power sharing performance of MGs. The dynamic response is promoted by suppressing the coupled power oscillations and power overshoots while realizing accurate power sharing. In addition, the proposed power sharing controller has a better parametric adaptability. The stability and dynamic performances are analyzed with a small-signal state-space model. Simulation and experimental results are presented to investigate the validity of the proposed scheme.

Key words: Microgrid, Droop control, Virtual impedance, Power sharing, Dynamic performance

I. INTRODUCTION

The microgrid (MG) is an important and promising concept to integrate a cluster of different types of distributed generation (DG) units, loads and energy-storage systems [1]. The development and extension of MGs are considered as an effective way to promote the development of traditional power grid towards future smart distribution grids [2]. An MG can operate in either the grid-connected mode or the autonomous islanding operation mode [3] [4]. In islanded MGs, a key technique for multiple DG units is how to properly share loads.

The droop control method is widely used to operate DG units in parallel. It can manage power sharing without communication. The improved droop controllers in [5]-[7] can realize accurate load sharing by measuring the common load voltage accurately. A Q-V dot droop method that improves reactive power sharing accuracy was presented in [8]. A virtual impedance optimization method for reactive power sharing in a networked MG was studied in [9], where a genetic algorithm was employed to optimize the parameters offline. A strategy using adaptive virtual impedance was proposed to improve reactive power sharing accuracy in [10].

In order to eliminate power sharing errors without knowledge of the feeder impedances, communication or control interconnection combined with primary droop control was studied in [11]-[21].

Recently, a modified droop method including power sharing error reduction operation and voltage recovery operation was proposed in [11]. A consensus-based distributed voltage control (DVC) that solves the problem of reactive power sharing under dominantly inductive power line conditions was studied in [12]. Integral controllers were employed to improve the power sharing accuracy by voltage

Manuscript received May 29, 2016; accepted Oct. 28, 2016
Recommended for publication by Associate Editor Il-Yop Chung.
†Corresponding Author: mahao@zju.edu.cn
Tel: +86-571-87953771, Zhejiang University
*College of Electrical Engineering, Zhejiang University, China
**College of Mechanical and Electrical Engineering, China Jiliang University, China

set-point regulation in [13]-[17].

The virtual impedance method can provide better performance than set-point regulation methods when communication is unavailable [18]. A virtual resistance, a virtual inductance and a virtual complex impedance variable tuned by an integrator are added in [18]-[20] to realize accurate reactive power sharing, respectively. In addition, an enhanced virtual impedance control approach using DG line current and point of common coupling (PCC) voltage feed-forward terms was proposed in [21]. A satisfactory power sharing accuracy can be obtained with the strategies in [11]-[21].

The real and reactive power can achieve satisfactory decoupling control with the droop method if the impedances of the DG units are resistive, inductive or even capacitive. For the DG units in an MG, long and mainly resistive feeders, interface reactors and/or transformers make the impedances more complex. Although the virtual impedance method has the ability to adjust the output impedance [22]-[27], it may be improper to tune the total impedance to be resistive, inductive or capacitive, because the required virtual impedance can be very large. Therefore, it is difficult to avoid coupling between real and reactive power in an MG.

This paper focuses on an improvement of the power sharing performance with the virtual impedance method. The existing virtual impedance methods consider virtual impedance for the voltage controlled power (VCP) (reactive power for Q-V droop, and real power for P-V droop) [18]-[21], which yields a 1-DOF (degree of freedom) tunable virtual impedance, since the sharing accuracy of the frequency controlled power (FCP) (real power for P-ω droop, and reactive power for Q-ω droop) can be guaranteed in the steady state regardless of impedances. However, it should be noted that a weak impedance matching for VCP sharing may lead to overshoots or even oscillations of the FCP under load variations, which results in FCP oscillations due to the strong coupling, especially when having an impedance with comparable reactance and resistance. Thus, the system stability is deteriorated.

On the basis of previous studies [18]-[21], a power sharing scheme based on adaptive virtual impedances, called the IM-PQ scheme, is proposed to improve the power sharing performance for islanded MGs in this paper. With P-V and Q-ω droop control, impedance matching for real power and reactive power sharing is considered, which yields 2-DOF tunable virtual impedances. Experimental results indicate that the dynamic response of the power sharing is promoted through restraining the coupled power oscillations while accurate power sharing is realized. Furthermore, the proposed power sharing controller has a better parametric adaptability. In addition, the system is robust to communication failures.

This paper is organized as follows. Power sharing based on impedance regulation is analyzed and the impedance matching concept is described in Section II. The details of the proposed scheme are discussed in Section III. Section IV presents an analysis of the DG output impedance and the small signal stability of the system with the proposed scheme. Simulation and experimental results are presented in Section V. Finally, some conclusions are drawn in Section VI.

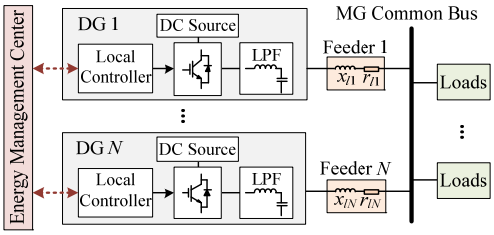

Fig. 1. Structure of an islanded MG system.

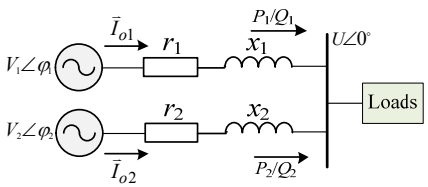

Fig. 2. Simplified model of an MG with two DG units.

II. Analysis of Power Sharing Based on Impedance Regulation

The structure of an islanded MG is shown in Fig. 1, consisting of a number of DG units and loads. The DG units are connected to the MG common bus through their respective feeders. Each DG unit can communicate with the MG energy management center (EMC) via the low-bandwidth communications link. Normally, the EMC works to achieve power management, high layer optimization and monitoring. If a fault occurs in the EMC, the MG should operate autonomously based on the primary droop control.

In the islanded mode, especially in the low voltage MGs, the DG unit can operate using Q-ω and P-V droop control as [1]:

$$V_i = V^* - k_{pi}P_i \tag{1}$$

$$\omega_i = \omega^* + k_{qi}Q_i \tag{2}$$

where V^* and ω^* are the nominal values of the output voltage amplitude and angular frequency, while V_i and ω_i are the set values. P_i and Q_i are the average fundamental real power and reactive power, and k_{pi} and k_{qi} are the voltage and angular frequency droop coefficients, respectively.

A simplified model with two DG units is analyzed, as depicted in Fig. 2, where V_i (i =1, 2) and U are the amplitudes of the inverter equivalent output voltage and the MG bus voltage, respectively; φ_i is the power angle; $\bar{I}_{oi}$ is the inverter output current; and r_i and x_i are the corresponding resistive and inductive component of the total impedance, which consists of the DG equivalent output impedance, virtual impedance, feeder impedance, interface reactors and/or

transformers.

With Q-ω and P-V droop control, the reactive power sharing is always accurate in the steady state owing to the global grid frequency. Hence, the reactive power sharing $Q_1 = mQ_2$ can be guaranteed as long as the angular frequency droop coefficients are chosen as $k_{q2} = mk_{q1}$. However, the real power sharing accuracy is poor under mismatched impedances. Next, the condition of $P_1 = nP_2$ under complex impedances is analyzed and the conclusions are given.

A. Real Power Sharing Analysis

According to Fig. 2, the complex power of the DG i flowing into the MG bus is:

$$\bar{S}_i = \bar{U} \cdot \bar{I}_{oi}^{\ *} = P_i + jQ_i \tag{3}$$

where $\bar{I}_{oi}^{\ *}$ is the conjugate of $\bar{I}_{oi}$. By substituting $\bar{I}_{oi} = (V_i \angle \varphi_i - U)/(r_i + jx_i)$ into (3), the real power and reactive power can be calculated as:

$$P_i = \frac{(r_i \cos\varphi_i + x_i \sin\varphi_i)UV_i - U^2 r_i}{r_i^2 + x_i^2} \tag{4}$$

$$Q_i = \frac{(x_i \cos\varphi_i - r_i \sin\varphi_i)UV_i - U^2 x_i}{r_i^2 + x_i^2} \tag{5}$$

Substituting (1) into (4), the real power of the inverter can be obtained as:

$$P_i = \frac{(r_i \cos\varphi_i + x_i \sin\varphi_i)UV^* - U^2 r_i}{r_i^2 + x_i^2 + k_{pi}U(\cos r_i + x_i \sin\varphi_i)} \tag{6}$$

Substituting (6) into (1) yields:

$$V_i = V^* - \frac{UV^* + \dfrac{U^2 r_i}{(r_i \cos\varphi_i + x_i \sin\varphi_i)}}{\dfrac{r_i^2 + x_i^2}{k_{pi}(r_i \cos\varphi_i + x_i \sin\varphi_i)} + U} \tag{7}$$

In order to achieve $P_1 = nP_2$, the voltage droop coefficients are set as $k_{p2} = nk_{p1}$. According to (1), the voltage deviation $\Delta V = V_2 - V_1$ should be zero. From (7), the condition is satisfied if:

$$\begin{cases} \dfrac{r_1}{r_1 \cos\varphi_1 + x_1 \sin\varphi_1} = \dfrac{r_2}{r_2 \cos\varphi_2 + x_2 \sin\varphi_2} \\ \dfrac{r_1^2 + x_1^2}{r_1 \cos\varphi_1 + x_1 \sin\varphi_1} = \dfrac{r_2^2 + x_2^2}{n(r_2 \cos\varphi_2 + x_2 \sin\varphi_2)} \end{cases} \tag{8}$$

By observing (8), it is easy to know that one set of solutions is:

$$\begin{cases} r_2 = nr_1 \\ x_2 = nx_1 \\ \varphi_2 = \varphi_1 \end{cases} \tag{9}$$

This set of conditions is very strict, which is sufficient but not necessary. Define $r_2 = ar_1$, $x_2 = bx_1$, $\varphi_2 = c\varphi_1$ and $D_i = r_i/x_i$ and substitute them into (8). It can then be derived that:

$$\begin{cases} a = f_{\varphi,D_1} \cdot b \\ b = \dfrac{n(1 + D_1^2) \cdot f_{\varphi,D_1}}{1 + D_1^2 \cdot f_{\varphi,D_1}^{\ 2}} \end{cases} \tag{10}$$

where:

$$f_{\varphi,D_1} = \frac{\sin\varphi_2}{D_1 \cos\varphi_1 + \sin\varphi_1 - D_1 \cos\varphi_2} = f(\varphi_1, \varphi_2, D_1) \tag{11}$$

Equations (10) and (11) present the conditions of accurate real power sharing with complex total impedances using the Q-ω and P-V droop methods. The conditions are derived from zero voltage amplitude deviation. However, they contain the voltage phases of the parallel DG units, which indicate that coupling exists between the real power and the reactive power.

Furthermore, it can be seen from (10) and (11) that with a fixed set of parameters φ_1, φ_2 and n, there are infinite sets of a, b that will satisfy (10) for DG2 to achieve $P_1 = nP_2$, since there is an infinite number of D_1. Further, DG2 can achieve the required real power sharing ratio by only adjusting r_2 and x_2, and vice versa from the perspective of DG1. Note that the changes in the impedance of parallel units can lead to variations of φ_1 and φ_2 in the steady state.

B. Impedance Matching for Real and Reactive Power Sharing

Assume that an MG system consists of N DG units and that their respective total impedances are (Z_{10}, Z_{20}, ⋯, Z_{N0}). In addition, the objective ratio of the real power sharing is (P_{1i}: P_{2i}: ⋯: $P_{Ni} = n_{1i}$: n_{2i}: ⋯: n_{Ni}), denoted as O_{pi}. In order to achieve the power sharing objective O_{pi} under loads $Load_i$, the impedances are tuned to (Z_{11}, Z_{21}, ⋯, Z_{N1}) with the impedance regulation method. This array of impedances (Z_{11}, Z_{21}, ⋯, Z_{N1}) is defined as a group of matched impedances under the conditions of the real power sharing objective O_{pi} and loads $Load_i$. For real power sharing, the virtual impedance method can change the matches of the impedances between the DG units to improve the real sharing accuracy. When the loads change, the matched impedances are tuned to new values. If a communication failure occurs, the power sharing is not affected, and the power sharing error will be decreased after the load change. This is because the impedance matching for real power sharing between the DG units is improved.

For reactive power sharing, owing to the global frequency, its sharing accuracy is guaranteed in the steady state regardless of the impedances. Thus, the existing methods do not consider impedance matching for reactive power sharing. However, as shown in (5), instantaneous reactive power is affected by the impedance. Although it is filtered by a low pass filter, reactive power overshoots or even oscillations still exist under load variations when the impedance matching for the reactive power sharing is poor. This leads to real power oscillations due to coupling between real and reactive power, which deteriorates the system stability. Therefore, in order to restrain the reactive power overshoots and oscillations during reactive power demand variations, the impedance matching for reactive power sharing should be noticed and considered.

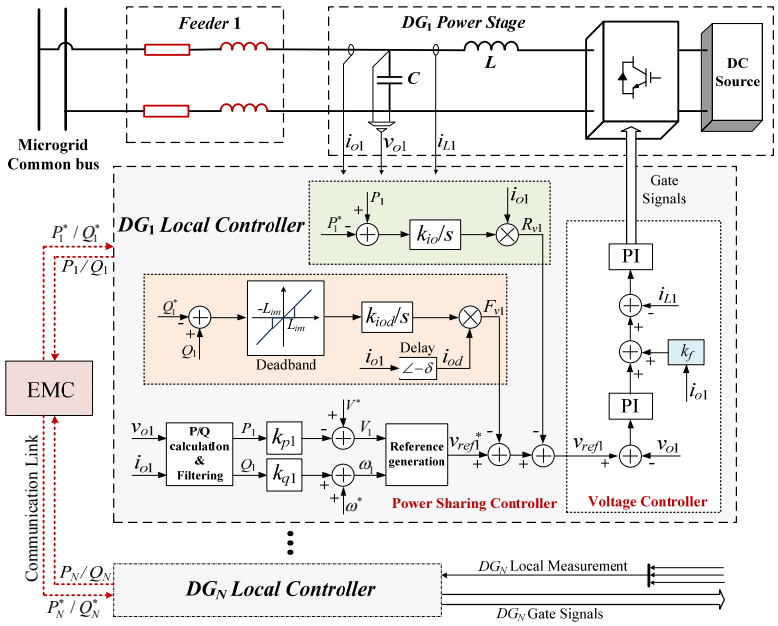

Fig. 3. Proposed overall control block diagram of the DG unit.

III. PROPOSED POWER SHARING SCHEME

There exists a strong coupling between real and reactive powers owing to the complex impedance property of DG units. Given this, in order to find a way to improve the dynamic response of the power sharing of MGs by suppressing the coupled power oscillations and power overshoots, information on both the real and reactive power should be used to adjust the virtual impedances. A simple power sharing scheme with two virtual impedance variables is proposed to improve the impedance matching for both the real and reactive power sharing between DG units in this section. It is 2-DOF tunable in impedance regulation for the power sharing control. The overall control block diagram of a DG unit in an MG is pictured in Fig. 3, including the power sharing controller and the voltage controller.

A. 2-DOF Tunable Adaptive Virtual Impedance Loop

As shown in Fig. 3, each DG unit sends its power to the EMC, and the EMC calculates the optimal power references and sends them back to the local controller of each DG, which can be calculated as:

$$\begin{cases} P_i^* = g_{pi} \sum_{j=1}^{N} P_j \\ Q_i^* = g_{qi} \sum_{j=1}^{N} Q_j \end{cases} \tag{12}$$

where g_{pi} and g_{qi} are the distribution coefficients of the DG i for the real and reactive power sharing, respectively.

To eliminate real power sharing errors, an adaptive virtual resistance tuned by an integrator using real power deviation can be used as:

$$R_{vi} = k_{io} \int (P_i - P_i^*)\, dt \tag{13}$$

where R_{vi} is the virtual resistance, k_{io} is the integral gain, and P_i^* is the power reference received from the EMC. According to equation (13), the DG unit providing more real power leads to a larger virtual resistance R_{vi}. This decreases the output real power, which improves the impedance matching for real power sharing. The real power will be equal to its reference in the steady state.

As previously mentioned, a weak impedance matching for reactive power sharing may result in reactive power overshoots and even oscillations, which will cause real power oscillations due to the strong coupling. To improve the impedance matching for reactive power sharing among the DG units, reactive power information is utilized to tune a virtual complex impedance variable as:

$$F_{vi} = k_{iod} \int (Q_i - Q_i^*)\, dt \tag{14}$$

where F_{vi} is the virtual impedance variable, k_{iod} is the integral gain, and Q_i^* is the power reference received from the EMC.

The proposed 2-DOF tunable adaptive virtual impedance method improves the matches of the impedances between the DG units. Not only the match between the impedances and the real power sharing but also the match between the impedances and the reactive power sharing is promoted. Thus, the reactive power overshoots and oscillations at the transients can be suppressed, which further promotes the dynamic performance of real power sharing due to the strong coupling.

It is noteworthy that the integral operation in equation (14) needs a deadband in the experiment. As illustrated in Fig. 3, the reactive power deviation is integrated only when its absolute value $|Q_i\text{-}Q_i^*|$ is greater than the pre-set limit L_{im}. The

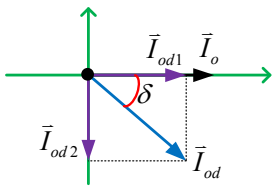

Fig. 4. Vector graphics of output current and delayed output current.

reason is twofold. First, the clock error, sampling error and power calculation error result in different calculated values of the reactive power among the DG units. However, the frequency is the same for all of the DG units in the steady state. As a result, the value of $(Q_i\text{-}Q_i^*)$ cannot reach zero and the integral operation continues until its output is equal to the limit value, which leads to an imbalance of the power sharing. Second, the real power sharing is accurate in the steady state due to the global frequency. Therefore, the integral operation in the steady state is inoperative. The limit value L_{im} should be greater than the amplitude of the ripple of the calculated reactive power, which is related to the steady state performance of the power sharing, the sampling precision and the power calculation method.

In this paper, for convenience of description, the method considering the impedance matching for only the real power sharing (only R_{vi} is added) is called the IM-P method. In addition, the 2-DOF tunable scheme (R_{vi} and F_{vi} are added) considering the impedance matching for both the real and reactive power sharing is called the IM-PQ scheme.

Note that the ripples of information transmitted through the communications link should be small enough due to the consideration of system stability. A moving average filter is recommended here [17].

B. Virtual Complex Impedance Implementation with the Current-Delay Method

As shown in Fig. 3, the virtual impedances consist of two parts: the virtual resistance R_v and the virtual complex impedance variable F_v. The reference voltage can be expressed as:

$$v_{ref} = v_{ref}^* - R_v i_o - F_v i_{od} \tag{15}$$

where v_{ref}* (v_{ref}*=$V\sin\omega t$) is the initial reference voltage produced by the droop control.

The virtual complex impedance is produced by the feedback of the delayed output current i_{od} with the delay angle δ. As shown in Fig. 4, the current vector $\bar{I}_{od}$ can be decomposed into two components: $\bar{I}_{od1}$ having the same phase as $\bar{I}_o$, and $\bar{I}_{od2}$ being orthogonal to $\bar{I}_o$. Define $\bar{I}_o$=$I_o\angle 0°$. Then, the current vector $\bar{I}_{od}$ can be expressed as:

$$\bar{I}_{od} = I_o\angle -\delta = \cos\delta \cdot I_o\angle 0^\circ - \sin\delta \cdot I_o\angle 90^\circ \tag{16}$$

According to (15) and (16), the added total virtual impedance Z_v can be obtained as:

$$Z_v = r_v + jx_v = R_v + F_v\cos\delta - jF_v\sin\delta \tag{17}$$

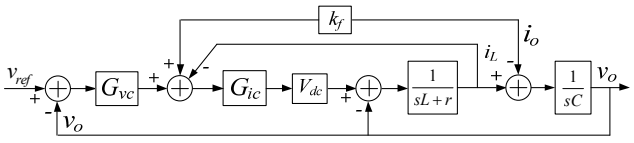

Fig. 5. Voltage controller of DG unit in an MG.

Using the current-delay method, a virtual inductor or capacitor, determined by the negative or positive F_v, can be produced without the differential operation, which has a high sensitivity to noises.

IV. Impedance Analysis and Modeling

A. Equivalent Output Impedance of DG Unit

According to Fig. 3, the voltage controller of a DG unit can be drawn as shown in Fig. 5. The proportional feedforward of the output current is introduced into the classical dual-loop control. V_{dc} is the input dc voltage, L and C are the output filter inductor and capacitor, r is the equivalent series resistance (ESR) of L and the on resistance of the switches, k_f is the feedforward coefficient of the output current, and i_L is the inductance current. The impact of the proportional feedforward of the output current on the equivalent impedance of the DG unit is explored.

Based on Thevenin's Theorem, an inverter behaves as a controlled voltage source with a voltage gain $G_c(s)$ and an output impedance $Z_o(s)$. According to Fig. 5, the output voltage can be derived as:

$$v_o = G_c(s)\cdot v_{ref} - Z_o(s)\cdot i_o \tag{18}$$

The expression of the output impedance $Z_o(s)$ is:

$$Z_o(s) = \frac{sL + r + (1-k_f)G_{ic}V_{dc}}{LCs^2 + rCs + CG_{ic}V_{dc}s + G_{vc}G_{ic}V_{dc} + 1} \tag{19}$$

where $G_{vc} = k_{pv}+k_{iv}/s$ and $G_{ic} = k_{pi}+k_{ii}/s$. Furthermore, k_{pv}, k_{iv}, k_{pi} and k_{ii} are the proportional and integral coefficients of voltage and current loop, respectively.

Using the parameters listed in Table I, the characteristic of $Z_o(s)$ is studied with different values of k_f (k_f=0, 0.7, 1 and 2), as illustrated in Fig. 6. It can be seen that the current feedforward coefficient has a significant impact on the characteristic of the output impedance $Z_o(s)$. Without the feedforward, i.e., when k_f=0, Z_o is large (8.49dB) and close to an inductance (86.1°) at the fundamental frequency. When k_f =0.7, the magnitude of Z_o is reduced to -1.86dB and the phase is 90.3°. In addition, when k_f =1, the magnitude of Z_o is further decreased to -21.5dB with a phase of 171°, having the negatively resistive characteristic. Furthermore, if k_f=2, Z_o is close to a capacitance with a magnitude of 8.48dB and a phase of 262°. In summary, the output impedance can be designed to be inductive, negatively resistive and capacitive with the proportional feedforward of the output current. In order to test the performance of the proposed scheme, k_f is intentionally selected as 0.7. It produces an inductive output

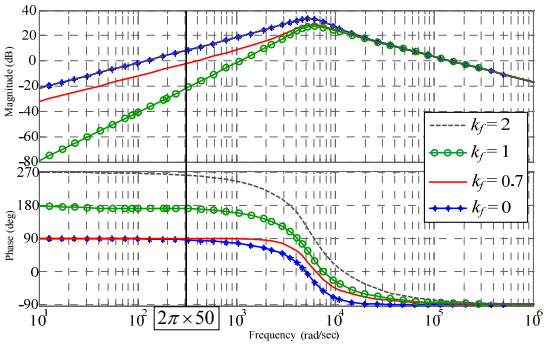

Fig. 6. Bode diagram of Z_o with different k_f (k_f = 0, 0.7, 1 and 2).

TABLE I
CIRCUIT AND CONTROL PARAMETERS

Input DC Voltage	V_{dc} =380V
Rated output voltage	V^*=311V
Filter Inductor	L =3.8mH
Filter Capacitor	C =6.8μF
ESR of Inductor L	r = 0.3Ω
Fundamental Frequency	f =50Hz
Switching Frequency	f_s =20kHz
PI Coefficients of Voltage Loop	k_{pv} =0.01; k_{iv} =120
PI Coefficients of Current Loop	k_{pi} =0.1; k_{ii} =6
Output Current Feedforward Coefficient	k_f =0.7
P-V Droop Coefficient	k_p =0.001V/W
Q-ω Boost Coefficient	k_q =0.0008(rad/s)/Var
Integral Gains	k_{io} =0.06; k_{iod} =0.1
Cutoff Frequency of Low-pass Filter	ω_c =20π rad/s
Delay Angle	δ =27°
Limit Value of $\lvert Q_i$-$Q_i^*\rvert$ for Integration	L_{im} =8W
Update Period of Communication	20 ms

impedance (j0.8Ω at the fundamental frequency), which makes the condition more severe with the Q-ω and P-V droop method.

B. Dynamic and Stability Performance

The stability and dynamic performance of a system with the IM-P and IM-PQ methods are analyzed and compared with the small-signal state-space model following the modeling approach in [14], [28].

Considering a non-stiff MG bus voltage and modeling of the low-pass filter with a first-order approximation, the small-signal variations of the real and reactive powers can be obtained as:

$$\Delta P_i = \frac{\omega_c}{s+\omega_c}\sum_{j=1}^{N}\left(\frac{\partial P_i}{\partial \varphi_j}\Delta\varphi_j + \frac{\partial P_i}{\partial V_j}\Delta V_j + \frac{\partial P_i}{\partial r_j}\Delta r_j + \frac{\partial P_i}{\partial x_j}\Delta x_j\right) \quad (20)$$

$$\Delta Q_i = \frac{\omega_c}{s+\omega_c}\sum_{j=1}^{N}\left(\frac{\partial Q_i}{\partial \varphi_j}\Delta\varphi_j + \frac{\partial Q_i}{\partial V_j}\Delta V_j + \frac{\partial Q_i}{\partial r_j}\Delta r_j + \frac{\partial Q_i}{\partial x_j}\Delta x_j\right) \quad (21)$$

where the operator Δ denotes a small-signal disturbance around the DG system equilibrium point, and ω_c is the cutoff angular frequency of the low-pass filter.

Using (13), (14) and (17), the disturbances of the resistance and inductance can be obtained as:

$$\Delta\dot{r}_i = k_{io}\left(\Delta P_i - g_{pi}\sum_{j=1}^{N}\Delta P_j\right) + k_{iod}\cos\delta\left(\Delta Q_i - g_{qi}\sum_{j=1}^{N}\Delta Q_j\right) \quad (22)$$

$$\Delta\dot{x}_i = -k_{iod}\sin\delta\left(\Delta Q_i - g_{qi}\sum_{j=1}^{N}\Delta Q_j\right) \quad (23)$$

Perturbing (1) and (2) yields:

$$\Delta V_i = -k_{pi}\Delta P_i \quad (24)$$

$$\Delta\omega_i = k_{qi}\Delta Q_i \quad (25)$$

With $\Delta\omega_i = s\Delta\varphi_i$ and (20)-(25), the small-signal state-space model of the proposed IM-PQ scheme can be derived as:

$$\dot{\boldsymbol{x}}_{MG}(t) = \boldsymbol{A}_{MG}\boldsymbol{x}_{MG}(t) \quad (26)$$

where the state variables are $\boldsymbol{x}_{MG}$=[ΔP_1, ΔP_2, ⋯, ΔP_N, ΔQ_1, ΔQ_2, ⋯, ΔQ_N, $\Delta\varphi_1$, $\Delta\varphi_2$, ⋯, $\Delta\varphi_N$, Δr_1, Δr_2, ⋯, Δr_N, Δx_1, Δx_2, ⋯, Δx_N]^T, which includes 5N state variables. The state-space model of the DG unit with the IM-P method can be obtained by substituting k_{iod} =0 into (26). Note that the order of a system with the IM-PQ scheme does not increase compared with that using the IM-P method. The detailed expression of A_{MG} is shown in the Appendix.

An islanded MG system with two identical DG units is investigated to evaluate the proposed scheme. The system parameters are listed in Table I. The inverter output impedance is j0.8Ω and the feeder impedances are set as r_{l1} = 1.1Ω, x_{l1} = 1.3mH, r_{l2} = 0.6Ω, and x_{l2} = 0.7mH. The dynamic and stability performance of the system with varied control parameters are given and compared.

Fig. 7(a) shows the root locus of the system with the IM-P method with a varied Q-ω boost slope k_q, which changes from 0.0002 (rad/s)/W to 0.004(rad/s)/W. There are four zero eigenvalues λ_1, λ_2, λ_3 and λ_4 due to the singularity of the state matrix $\boldsymbol{A}_{MG}$. The dominate poles λ_5 and λ_6 gradually become underdamped, which leads to a more oscillatory response. As shown in Fig. 7(b), when the virtual impedance variable F_v is added, it can be seen that λ_5 and λ_6 are further away from the imaginary axis and less sensitive to variations of k_q, which represents the enhanced dynamic and stability performance of the system with the IM-PQ scheme.

Fig. 8(a) shows the root locus of the IM-P method with a varied integral gain k_{io}. When k_{io} increases, λ_7 moves leftward on the real axis and becomes a complex number with λ_8 being its conjugate. Meanwhile, λ_5 and λ_6 move towards the imaginary axis. At first, the system obtains an improved dynamic response but later becomes more oscillatory. To maintain proper stability and damping features, the selected gain k_{io} is 0.015. The corresponding operation point is marked with "x" in the root locus diagrams. When the impedance matching for the reactive power sharing is considered, namely, when F_v is added, λ_5 and λ_6 are not sensitive to variations of k_{io} and more far away from the imaginary axis, as shown in Fig. 8(b). This shows that the IM-PQ scheme is more robust than the IM-P method. In order to obtain satisfied system damping and stability performance,

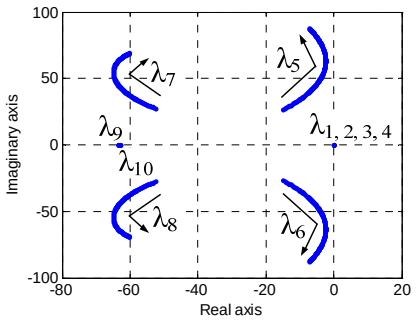

(a) With IM-P method.

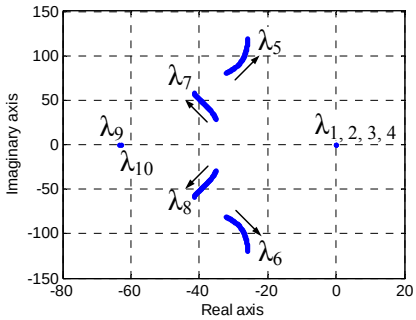

(b) With IM-PQ scheme.

Fig. 7. Root locus diagrams with varied k_q: $0.0002 \le k_q \le 0.004$. (a) With IM-P method. (b) With IM-PQ scheme.

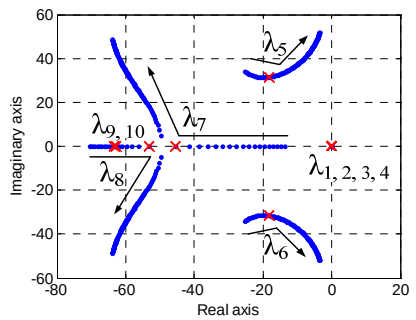

(a) With IM-P method.

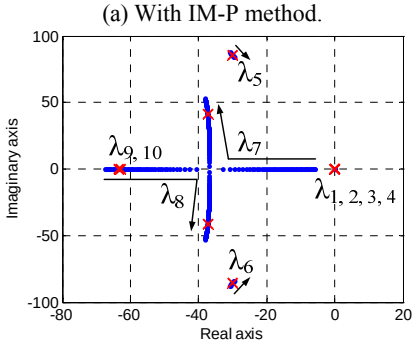

(b) With IM-PQ scheme.

Fig. 8. Root locus diagrams with variation in integral gain k_{io}: $0.008 \le k_{io} \le 0.08$. (a) With IM-P method. (b) With IM-PQ scheme.

the integral gain k_{io} is selected as 0.06 for the IM-PQ scheme.

The root locus diagram with a varied parameter k_{iod} is given in Fig. 9. The dominant eigenvalues λ_5 and λ_6 move from the right to the left while λ_7 and λ_8 move towards the imaginary axis, indicating that the stability and dynamic performance of the system is improved with an increased k_{iod} within a certain range. The designed eigenvalues are marked by "x" with an integral gain of $k_{iod} = 0.1$.

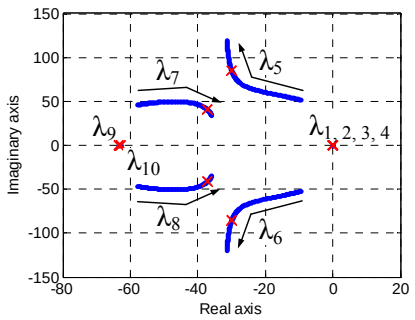

Fig. 9. Root locus diagram with variation in integral gain k_{iod} using the proposed IM-PQ scheme: $0.02 \le k_{iod} \le 0.2$.

TABLE II
SIMULATION PARAMETERS

Feeder impedance	Feeder 1: 1.1Ω + 1.3mH Feeder 2: 0.6Ω + 0.7mH Feeder 3: 0.9Ω + 0.7mH
Integral Gains	$k_{io1} = k_{io2} = 2k_{io3} = 0.06$ $k_{iod1} = k_{iod2} = 2k_{iod3} = 0.1$
P-V Droop Coefficient	$k_{p1} = k_{p2} = 2k_{p3} = 0.001$V/W
Q-ω Boost Coefficient	$k_{q1} = k_{q2} = 2k_{q3} = 0.0008$(rad/s)/Var

V. SIMULATION AND EXPERIMENTAL RESULTS

A. Simulation Verification

To verify the proposed control scheme, a simulation model composed of three DG units was built in the PLECS environment. Each DG unit employs the proposed control method as show in Fig. 3, and uses the control parameters listed in Table I. Three DG units are intended to achieve 1:1:2 power sharing. The respective integral gains and droop coefficients are listed in Table II, including the feeder impedances. The stage (*stage-a*) from the start of the compensation to the elimination of the power sharing error is concerned. This transient can be seen as the power distribution process of an MG, in which the power sharing ratio changes.

The simulated power sharing performances are shown in Fig. 10. At the beginning, the conventional droop control is used. It can be seen that the real power sharing accuracy is poor while the reactive power sharing is accurate. Then the power sharing compensation is enabled. Fig. 10(a) shows the performance of the IM-P method. The regulation time in *stage-a* takes 0.65 s with a slight real power overshoot in the real power. If the integral gain k_{io} increases, it will lead to power oscillations and extend the regulating time. Fig. 10(b) presents simulated result of the proposed IM-PQ scheme. The duration time in *stage-a* is reduced to 0.20 s. The simulation results show that the MG obtains a faster dynamic response of the power sharing with the proposed IM-PQ scheme.

B. Experimental Results

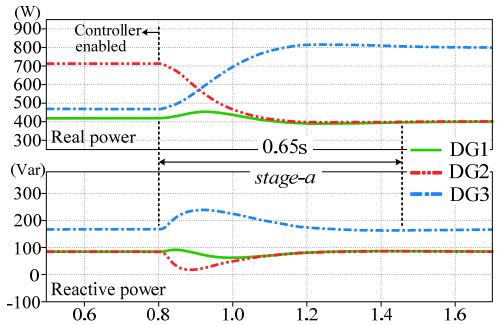

(a) With IM-P method.

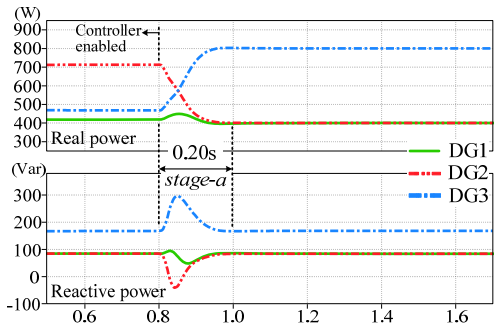

(b) With IM-PQ scheme.

Fig. 10. Simulated power sharing performance. (a) With IM-P method. (b) With IM-PQ scheme.

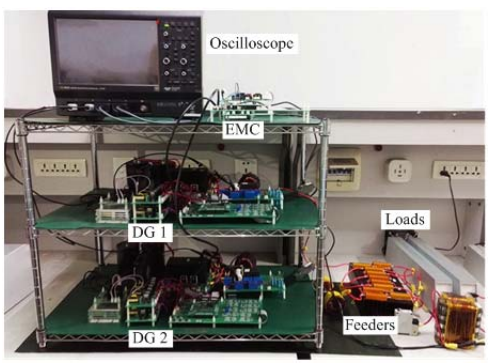

Fig. 11. Experiment setup.

An MG prototype with two DG units is built in the laboratory, as shown in Fig. 11. The circuit and control parameters are listed in Table I. The feeder impedances are selected to be the same as feeder 1 and feeder 2 in Table II. Both of the DG units are controlled by a TMS320F28335 (DSP). The CAN bus is used as a communications link. Without a loss of generality, the same power ratio is considered. In addition, *stage-a*, *stage-b* (the loads step up) and *stage-c* (the loads step down) are emphasized to evaluate the performance of the control method.

1) Performance of the Conventional Droop Method: The power sharing results of the conventional Q-ω and P-V droop methods (k_{io} = k_{iod} = 0 in Fig. 3) with load variations are shown in Fig. 12. The reactive power sharing is accurate due to the global frequency. However, there exist significant sharing errors in the real power sharing owing to the mismatch of the feeder impedances. Moreover, there are

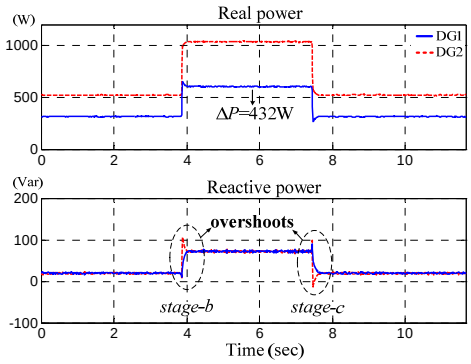

Fig. 12. Experimental power sharing performance of conventional droop control method.

measurable reactive power overshoots at the load changes. This fact indicates that the current impedance matching for the reactive power sharing is weak.

2) Performance of the IM-P Method: The power sharing performance of the IM-P method is presented in Fig. 13. With an optimized integral gain k_{io} (k_{io}=0.015), the duration in *stage-a* is 0.37 s with slight oscillations at the load variations, as shown in Fig. 13(a). Since the IM-P method does not directly improve the impedance matching for the reactive power sharing, the improvement of the reactive power overshoots under load changes is not obvious when compared with Fig. 12. In addition, the three regulation processes oscillate when an increased k_{io} (k_{io}=0.06) is used, with a duration of 0.58 s in *stage-a*, as shown in Fig. 13(b). These results indicate that when a larger integral gain is adopted for the purpose of improving the dynamic response, the power oscillates, which extends the regulating time.

Fig. 14 presents the power sharing results with increased droop coefficients (k_q=0.004, k_p=0.0015). It can be seen that the dynamic in *stage-a* (0.17 s) is faster than that in Fig. 13. However, the power oscillations are significant even in the steady state, which shows a way to enhance the power dynamics by increasing the droop gains exacerbate system stability, especially when the ratio of the total reactance to the resistance is considerable [28].

3) Performance of the Proposed IM-PQ Scheme: The power sharing results of the proposed IM-PQ scheme with different delay angles are shown in Fig. 15. Compared with Fig. 13, the power sharing performance is better when a virtual resistance F_v (δ=0º) is adopted, as shown in Fig. 15(a). The duration of *stage-a* is reduced to 0.14 s. The power overshoots in *stage-b* and *stage-c* are decreased to a certain extent, and the regulating processes are smoother. When F_v is added as a complex impedance variable with a delay angle of 27º, the performance of power sharing is further improved. As shown in Fig. 15(b), the time of *stage-a* is reduced to 0.12 s. In addition, the transient processes in *stage-b* and *stage-c* are almost negligible and the power overshoots are basically eliminated. Note that the integral gain k_{io} (k_{io}=0.06) is the same as that in Fig. 13(b).

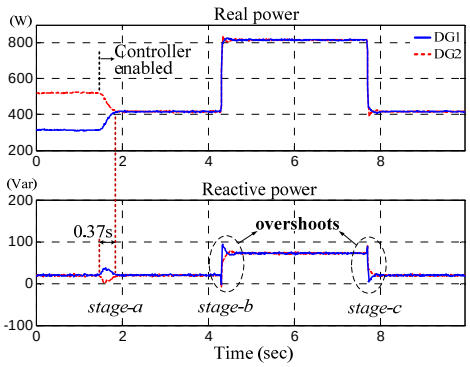

(a) k_{io}=0.015.

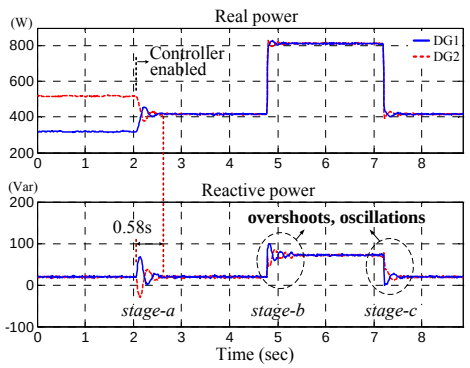

(b) k_{io}=0.06.

Fig. 13. Experimental power sharing results of the IM-P method with different k_{io}.

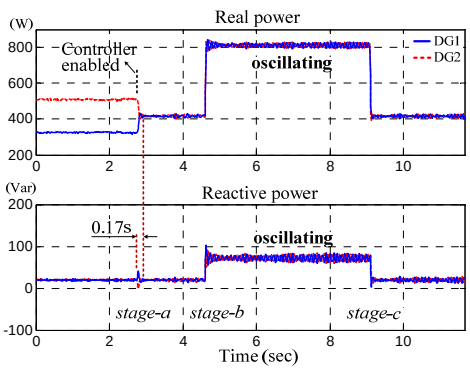

Fig. 14. Experimental power sharing results of the IM-P method with increased droop coefficients: k_q=0.004, k_p=0.0015.

To visually show the performance of the proposed IM-PQ scheme, the DG currents and their difference values in the three stages are presented in Fig. 16. It can be seen that the current regulation is fast and smooth in *stage-a* and that the difference value of output currents during load variations is ripple-free, which shows the enhanced dynamic performance of power sharing with the IM-PQ scheme.

When increased droop coefficients (k_q=0.004, k_p=0.0015) are used, the performance of the IM-PQ scheme is presented in Fig. 17(a). The dynamic in *stage-a* is faster with a duration of 0.07 s while the power oscillations are well suppressed, in contrast to the result of the IM-P method shown in Fig. 14. In addition, Fig. 17(b) presents real-time tuning of the added virtual impedances. Although the complex impedance

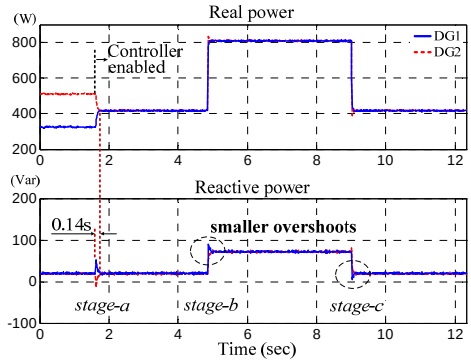

(a) δ=0º.

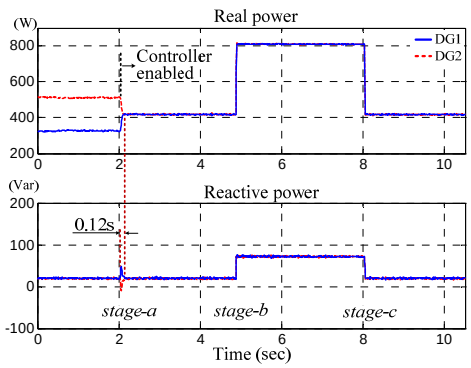

(b) δ=27º.

Fig. 15. Experimental power sharing results of the proposed IM-PQ scheme with different delay angle δ.

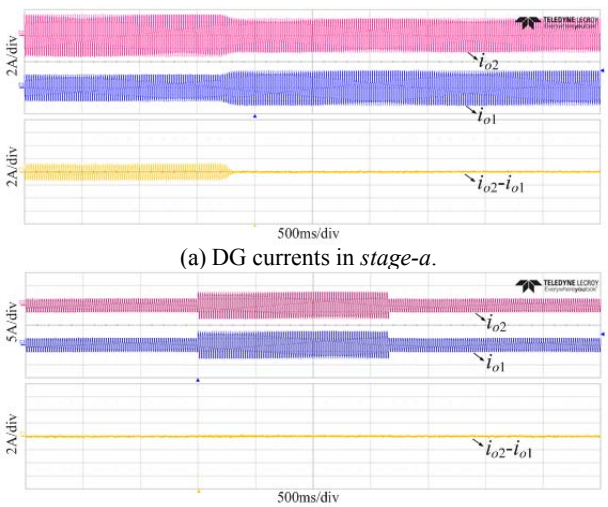

(a) DG currents in *stage-a*.

(b) DG currents in *stage-b* and *stage-c*.

Fig. 16. Experimental waveforms of output currents with the proposed IM-PQ scheme.

variable F_v is small, it does improve the matches of the total impedances.

Experimental results indicate that the proposed IM-PQ scheme improves the dynamic responses of the power sharing and enhances the system stability by suppressing the coupled power oscillations and reactive power overshoots. Moreover, the parameter adaptation of the IM-PQ scheme is better than that of the IM-P method. Better power sharing performance is provided by improving the impedance matching for both the

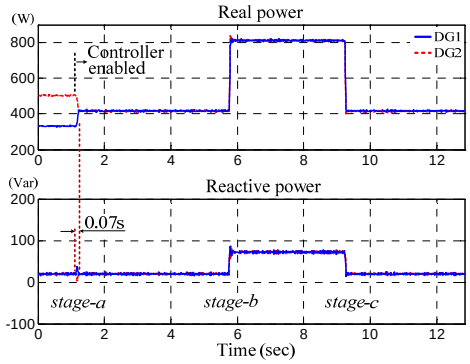

(a) Power sharing.

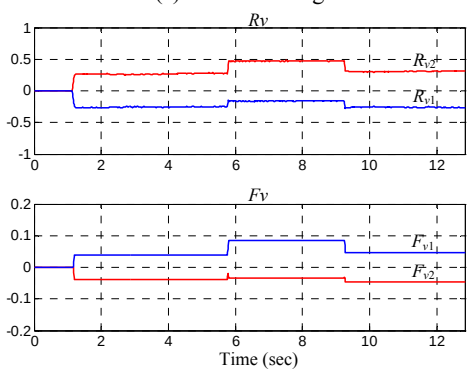

(b) Virtual impedance variables.

Fig. 17. Experimental result of the IM-PQ scheme with increased droop coefficients: k_q=0.004, k_p=0.0015.

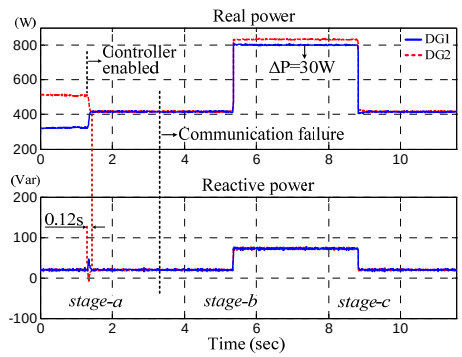

Fig. 18. Experimental power sharing of the IM-PQ scheme with a communication failure.

real and reactive power sharing. In addition, a small inductive or capacitive component in F_v results in better matched impedances than a pure resistive F_v.

4) Performance of the IM-PQ Scheme with Communication Failures: To verify the power sharing performance of the IM-PQ scheme with a communication interruption, the communication lines connected to the EMC are manually unplugged. When the DG unit detects a communication timeout, the integral operations are stopped and R_v and F_v are held at its last tuned values. The result is shown in Fig. 18. It can be seen that the power sharing is unaffected if the load demands stay the same. In addition, when the load steps up, the real power sharing error ΔP is reduced from 432W to 30W and the reactive power overshoots under load variations are ignorable, comparing the result in Fig. 12 with the conventional droop control method.

VI. CONCLUSIONS

In this study, the power sharing of an MG with the Q-ω and P-V droop method is analyzed, and the concept of impedance matching for real and reactive power sharing is described. An IM-PQ scheme considering the impedance matching for both real and reactive power sharing is proposed. It includes two independent virtual impedance variables. The impact of the proportional feedforward of the output current on the equivalent output impedance of the DG unit is explored. In addition, a small signal model is built to investigate the dynamic and stability performance of the proposed strategy. The MG obtains accurate power sharing and an enhanced dynamic response with satisfactory suppression of the coupled power oscillations and reactive power overshoots. Meanwhile, the proposed method is robust to communication failures and it grants the power sharing controller a larger parameter adaptation. Finally, simulation and experimental results are presented to show the improved performance of the proposed scheme. These results are consistent with the reported theoretical analysis.

APPENDIX

The detailed expression of matrix A_{MG} in Equ. (26) is:

$$\boldsymbol{A}_{MG}=\begin{bmatrix} \boldsymbol{A}_{PP} & \boldsymbol{O}_{N\times N} & \omega_c\boldsymbol{A}_{P\varphi} & \omega_c\boldsymbol{A}_{Pr} & \omega_c\boldsymbol{A}_{Px} \\ \boldsymbol{A}_{QP} & -\omega_c\boldsymbol{I}_N & \omega_c\boldsymbol{A}_{Q\varphi} & \omega_c\boldsymbol{A}_{Qr} & \omega_c\boldsymbol{A}_{Qx} \\ \boldsymbol{O}_{N\times N} & \boldsymbol{K}_q & \boldsymbol{O}_{N\times N} & \boldsymbol{O}_{N\times N} & \boldsymbol{O}_{N\times N} \\ \boldsymbol{A}_{rP} & \boldsymbol{A}_{rQ} & \boldsymbol{O}_{N\times N} & \boldsymbol{O}_{N\times N} & \boldsymbol{O}_{N\times N} \\ \boldsymbol{O}_{N\times N} & \boldsymbol{A}_{xQ} & \boldsymbol{O}_{N\times N} & \boldsymbol{O}_{N\times N} & \boldsymbol{O}_{N\times N} \end{bmatrix}$$

where:

$$\boldsymbol{A}_{PP}=-\omega_c\boldsymbol{I}_N-\omega_c\begin{bmatrix} k_{p1}\dfrac{\partial P_1}{\partial V_1} & \cdots & k_{pN}\dfrac{\partial P_1}{\partial V_N} \\ \vdots & \ddots & \vdots \\ k_{p1}\dfrac{\partial P_N}{\partial V_1} & \cdots & k_{pN}\dfrac{\partial P_N}{\partial V_N} \end{bmatrix},$$

$$\boldsymbol{A}_{P\varphi}=\begin{bmatrix} \dfrac{\partial P_1}{\partial \varphi_1} & \cdots & \dfrac{\partial P_1}{\partial \varphi_N} \\ \vdots & \ddots & \vdots \\ \dfrac{\partial P_N}{\partial \varphi_1} & \cdots & \dfrac{\partial P_N}{\partial \varphi_N} \end{bmatrix},\quad \boldsymbol{A}_{Pr}=\begin{bmatrix} \dfrac{\partial P_1}{\partial r_1} & \cdots & \dfrac{\partial P_1}{\partial r_N} \\ \vdots & \ddots & \vdots \\ \dfrac{\partial P_N}{\partial r_1} & \cdots & \dfrac{\partial P_N}{\partial r_N} \end{bmatrix},$$

$$\boldsymbol{A}_{Px}=\begin{bmatrix} \dfrac{\partial P_1}{\partial x_1} & \cdots & \dfrac{\partial P_1}{\partial x_N} \\ \vdots & \ddots & \vdots \\ \dfrac{\partial P_N}{\partial x_1} & \cdots & \dfrac{\partial P_N}{\partial x_N} \end{bmatrix},\quad \boldsymbol{A}_{Q\varphi}=\begin{bmatrix} \dfrac{\partial Q_1}{\partial \varphi_1} & \cdots & \dfrac{\partial Q_1}{\partial \varphi_N} \\ \vdots & \ddots & \vdots \\ \dfrac{\partial Q_N}{\partial \varphi_1} & \cdots & \dfrac{\partial Q_N}{\partial \varphi_N} \end{bmatrix},$$

$$\boldsymbol{A}_{Qr}=\begin{bmatrix}\frac{\partial Q_1}{\partial r_1} & \cdots & \frac{\partial Q_1}{\partial r_N}\\ \vdots & \ddots & \vdots\\ \frac{\partial Q_N}{\partial r_1} & \cdots & \frac{\partial Q_N}{\partial r_N}\end{bmatrix},\quad \boldsymbol{A}_{Qx}=\begin{bmatrix}\frac{\partial Q_1}{\partial x_1} & \cdots & \frac{\partial Q_1}{\partial x_N}\\ \vdots & \ddots & \vdots\\ \frac{\partial Q_N}{\partial x_1} & \cdots & \frac{\partial Q_N}{\partial x_N}\end{bmatrix},$$

$$\boldsymbol{A}_{QP}=-\omega_c\begin{bmatrix}k_{p1}\frac{\partial Q_1}{\partial V_1} & \cdots & k_{pN}\frac{\partial Q_1}{\partial V_N}\\ \vdots & \ddots & \vdots\\ k_{p1}\frac{\partial Q_N}{\partial V_1} & \cdots & k_{pN}\frac{\partial Q_N}{\partial V_N}\end{bmatrix},$$

$$\boldsymbol{K}_q=\begin{bmatrix}k_{q1} & 0 & \cdots & 0\\ 0 & k_{q2} & \cdots & 0\\ \vdots & \vdots & \ddots & 0\\ 0 & 0 & 0 & k_{qN}\end{bmatrix},$$

$$\boldsymbol{A}_{rP}=k_{io}\boldsymbol{I}_N-k_{io}\begin{bmatrix}g_{p1} & \cdots & g_{p1}\\ \vdots & \ddots & \vdots\\ g_{pN} & \cdots & g_{pN}\end{bmatrix},$$

$$\boldsymbol{A}_{rQ}=k_{io}\cos\delta\cdot\boldsymbol{I}_N-k_{io}\cos\delta\begin{bmatrix}g_{q1} & \cdots & g_{q1}\\ \vdots & \ddots & \vdots\\ g_{qN} & \cdots & g_{qN}\end{bmatrix},$$

$$\boldsymbol{A}_{xQ}=-k_{iod}\sin\delta\cdot\boldsymbol{I}_N+k_{iod}\sin\delta\begin{bmatrix}g_{q1} & \cdots & g_{q1}\\ \vdots & \ddots & \vdots\\ g_{qN} & \cdots & g_{qN}\end{bmatrix},$$

$\boldsymbol{O}$ is the zero matrix, and $\boldsymbol{I}_N\in\boldsymbol{R}^{N\times N}$ is the identity matrix.

ACKNOWLEDGMENT

This project is supported by the National Natural Science Foundation of China (51177149), the Specialized Research Fund for the Doctoral Program of Higher Education (20130101110108), and the Key Laboratory of Electrical Equipment and System of Marine Renewable Energy in Zhejiang Province.

REFERENCES

[1] J. Rocabert, A. Luna, F. Blaabjerge, and P. Rodriguez, "Control of power converters in AC microgrids," *IEEE Trans. Power Electron.*, Vol. 27, No. 11, pp. 4734-4749, Nov. 2012.

[2] S. M. Ashabani, Y. A. I. Mohamed, "New family of microgrid control and management strategies in smart distribution grids – Analysis, comparison and testing," *IEEE Trans. Power Syst.*, Vol. 29, No. 5, pp. 2257-2269, Sep. 2014.

[3] J. M. Guerrero, J. C. Vasquez, J. Matas, L. G. de Vicuna, and M. Castilla, "Hierarchical control of droop-controlled AC and DC microgrids – A general approach toward standardization," *IEEE Trans. Ind. Electron.*, Vol. 58, No. 1, pp. 158-172, Jan. 2011.

[4] X. Wang, J. M. Guerrero, F. Blaabjerg, and Z. Chen, "A review of power electronics based microgrids," *Journal of Power Electronics*, Vol. 12, No. 1, pp. 181-192, Jan. 2012.

[5] C. K. Sao and P. W. Lehn, "Autonomous load sharing of voltage source converters," *IEEE Trans. Power Del.*, Vol. 20, No. 2, pp. 1009-1016, Apr. 2005.

[6] Q. C. Zhong, "Robust droop controller for accurate proportional load sharing among inverters operated in parallel," *IEEE Trans. Ind. Electron.*, Vol. 60, No. 4, pp. 1281-1290, Apr. 2013.

[7] X. Zhang, J. Liu, Z. You, and T. Liu, "Study on the influence of distribution lines to parallel inverter systems adopting the droop control method," *Journal of Power Electronics*, Vol. 13, No. 4, pp. 701-711, Jul. 2013.

[8] C.-T. Lee, C.-C. Chu, and P.-T. Cheng, "A new droop control method for the autonomous operation of distributed energy resource interface converters," *IEEE Trans. Power Electron.*, Vol. 28, No. 4, pp. 1980-1993, Apr. 2013.

[9] Y. Zhu, F. Zhuo, F. Wang, B. Liu, R. Gou, and Y. Zhao, "A virtual impedance optimization method for reactive power sharing in networked microgrid," *IEEE Trans. Power Electron.*, Vol. 31, No. 4, pp.2890-2904, Apr. 2016.

[10] Y. Zhu, F. Zhou, F. Wang, B. Liu, and Y. Zhao, "A wireless load sharing strategy for islanded microgrid based on feeder current sensing," *IEEE Trans. Power Electron.*. Vol. 30, No. 12, pp. 6706-6719, Dec. 2015.

[11] H. Han, Y. Sun, M. Su, and J. M. Guerrero, "An improved droop control strategy for reactive power sharing in islanded microgrid," *IEEE Trans. Power Electron.*, Vol.30, No.6, pp. 3133-3141, Jun. 2015.

[12] J. Schiffer, T. Seel, J. Raisch, and T. Sezi, "Voltage stability and reactive power sharing in inverter-based microgrids with consensus-based distributed voltage control," *IEEE Trans. Control Syst. Tech.*, Vol. 24, No. 1, pp.96-109, Jan. 2016.

[13] J. W. Simpson-Porco, Q. Shafiee, F. Dörfler, J. C. Vasquez, J. M. Guerrero, and F. Bullo, "Secondary frequency and voltage control of islanded microgrids via distributed averaging," *IEEE Trans. Ind. Electron.*, Vol. 62, No. 11, pp. 7025-7038, Nov. 2015.

[14] Q. Guo, H. Wu, L. Lin, Z. Bai, and H. Ma, "Secondary voltage control for reactive power sharing in an islanded microgrid," *Journal of Power Electronics*, Vol. 16, No. 1, pp. 329-339, Jan. 2016.

[15] Q. Shafiee, J. M. Guerrero, and J. C. Vasquez, "Distributed secondary control for islanded microgrids – A novel approach," *IEEE Trans. Power Electron.*, Vol. 29, No. 2, pp. 1018-1031, Feb. 2014.

[16] H. Mahmood, D. Michaelson, and J. Jiang, "Reactive power sharing in islanded microgrids using adaptive voltage droop control," *IEEE Trans. Smart Grid*, Vol. 6, No. 6, pp. 3052-3060, Nov. 2015.

[17] J. He and Y. W. Li, "An enhanced microgrid load demand sharing strategy," *IEEE Trans. Power Electron.*, Vol. 27, No.9, pp. 3984-3995, Sep. 2012.

[18] Y. Zhu, B. Liu, F. Wang, F. Zhuo, and Y. Zhao, "A virtual resistance based reactive power sharing strategy for networked microgrid," in *Proc. IEEE ICPE-ECCE Asia,* pp. 1564-1572, 2015.

[19] J. He, Y. W. Li, and F. Blaabjerg, "An enhanced islanding microgrid reactive power, imbalance power, and harmonic power sharing scheme," *IEEE Trans. Power Electron.*, Vol. 30, No. 6, pp. 3389-3401, Jun. 2015.

[20] H. Mahmood, D. Michaelson, and J. Jiang, "Accurate reactive power sharing in an islanded microgrid using

adaptive virtual impedances," *IEEE Trans. Power Electron.*, Vol. 30, No. 3, p. 1605-1617, Mar. 2015.
[21] J. He,Y. W. Li , J. M. Guerrero, F. Blaabjerg, and J. C. Vasquez, "An islanding microgrid power sharing approach using enhanced virtual impedance control scheme," *IEEE Trans. Power Electron.*, Vol. 28, No. 11, pp. 5272-5282, Nov. 2013.
[22] J. M. Guerrero, L G de Vicuña, J. Matas, M. Castilla, and J. Miret, "Output impedance design of parallel-connected UPS inverters with wireless load-sharing control," *IEEE Trans. Ind. Electron.*, Vol. 52, No.4, pp. 1126-1135, Aug. 2005.
[23] J. M. Guerrero, J. Matas, L G de Vicuña, M. Castilla, and J. Miret, "Wireless-control strategy for parallel operation of distributed-generation inverters," *IEEE Trans. Ind. Electron.*, Vol. 53, No. 5, pp. 1461-1470, Oct. 2006.
[24] J. M. Guerrero, J. Matas, L. G. de Vicuña, M. Castilla, and J. Miret, "Decentralized control for parallel operation of distributed generation inverters using resistive output impedance," *IEEE Trans. Ind. Electron.*, Vol. 54, No. 2, pp. 994-1004, Apr. 2007.
[25] W. Yao, M. Chen, J. M. Guerrero, and Z.-M. Qian, "Design and analysis of the droop control method for parallel inverters considering the impact of the complex impedance on the power sharing," *IEEE Trans. Ind. Electron.*, Vol. 58, No. 2, pp. 576-588, Feb. 2011.
[26] Q. C. Zhong and Y. Zeng, "Control of inverters via a virtual capacitor to achieve capacitive output impedance," *IEEE Trans. Power Electron.*, Vol. 29, No. 10, pp. 5568-5578, Oct. 2014.
[27] Z. Guo, D. Sha, and X. Liao, "Wireless paralleled control strategy of three-phase inverter modules for islanding distributed generation systems," *Journal of Power Electronics*, Vol. 13, No. 3, pp. 479-486, May 2013.
[28] A. Kahrobaeian and Y. A. I. Mohamed, "Networked-Based Hybrid Distributed Power Sharing and Control for Islanded Microgrid Systems," *IEEE Trans. Power Electron.*, Vol. 30, No. 2, pp. 603-617, Feb. 2015.

Liaoyuan Lin was born in Quanzhou, China. He received his B.S. degree in Electrical Engineering from Zhejiang University, Hangzhou, China, in 2012, where he is presently working towards his Ph.D. degree in Electrical Engineering. His current research interests include the control of inverters in UPS systems, distributed power generation and microgrids.

Qian Guo was born in Zhengzhou, China. She received her Ph.D. degree in Electrical Engineering from Zhejiang University, Hangzhou, China, in 2016. She is presently working as a Lecturer at the China Jiliang University, Hangzhou, China. Her current research interests include the control of inverters in microgrids and distributed generation systems.

Zhihong Bai was born in Shanxi, China. She received her Ph.D. degree in Electrical Engineering from Zhejiang University, Hangzhou, China, in 2008. Since 2011, she has been with Zhejiang University, where she is presently working as an Associate Professor in the College of Electrical Engineering. Her current research interests include renewable energy systems as well as high-power and multilevel converters.

Hao Ma was born in Hangzhou, China. He received his B.S., M.S., and Ph.D. degrees in Electrical Engineering from Zhejiang University, Hangzhou, China, in 1991, 1994, and 1997, respectively. He is presently working as a Professor in the College of Electrical Engineering, Zhejiang University. His current research interests include advanced control in power electronics, fault diagnosis of power electronic circuits and systems, and applications of power electronics.